JOURNAL OF SOLID STATE CHEMISTRY 92, 401–419 (1991)

A Study of the Decomposition of Praseodymium Hydroxy Carbonate and Praseodymium Carbonate Hydrate

RENU SHARMA,* HIROFUMI HINODE,† AND LEROY EYRING*,‡

Center for Solid State Science and ‡Department of Chemistry, Arizona State University, Tempe, Arizona 85287-1704

Received October 15, 1990; in revised form January 28, 1991

The decomposition reactions of praseodymium hydroxy carbonate and praseodymium carbonate octahydrate have been followed by thermogravimetric analysis, X-ray diffraction analysis of quenched, equilibrated specimens, *in situ* high temperature X-ray diffraction analysis, and dynamic *in situ* high-resolution electron microscopic observations. The decomposition reaction sequence for the praseodymium hydroxy carbonate includes the dioxymonocarbonate (three polymorphs) and various oxides depending on the conditions of the experiment. The decomposition reaction sequence for the carbonate hydrate includes a lower hydrate, the anhydrous carbonate, the three polymorphs of the dioxymonocarbonate, and various oxides again depending upon the conditions. The results of the various methods of study are presented and compared. While there is almost a quantitative agreement between the X-ray results, the correlation to the high-resolution electron microscopic results is qualitative. The similarities and differences are discussed. The most striking difference is the much lower temperatures of corresponding decompositions in the microscope.

Introduction

Modern high-voltage electron microscopes are capable of point-to-point resolution reaching 0.17 nm. These microscopes can be used to image fixed atomic arrangements even of great complexity. However, not all materials are stable in the high-voltage, high-flux electron beam. Indeed, most substances would decompose or transform into new materials or new structures under the effect of the electron beam. These instabilities can be utilized to study transformation or reaction mechanisms at the atomic level.

The rare earth oxides are of great importance in the ceramic industry where oxide entities are often fabricated by decomposing their carbonates, carbonate hydrates, hydroxy carbonates, or oxalates. There have been some thermogravimetric studies (TGA) (*1–4*) and even a high-temperature X-ray diffraction study (HTXRD) (*5*) of the hydroxy carbonate and the carbonate hydrate of praseodymium. We justify yet another study of this system by conducting the TGA at a slower rate of temperature increase, hence one nearer thermal equilibrium, doing more thorough HTXRD studies of the sequential reactions, and using high-resolution transmission electron microscopy (HRTEM) to observe the reactions at the atomic level *in situ*. It is this last reason

† Present address: Department of Chemical Engineering, Faculty of Engineering, Tokyo Institute of Technology, Tokyo 152, Japan.

0022-4596/91 $3.00

that most motivates the study since we wish to explore further the use of HRTEM in the study of chemical reaction mechanisms at the atomic level.

In a parallel study the corresponding neodymium carbonate system was investigated (*6*). A comparison of this previous work on neodymium compounds with that of the present will show similarities due the similar ionic radii of the trivalent cations and the differences caused by the lower oxidation potential of Pr^{3+} to become Pr^{4+}.

This multifaceted study was undertaken in order to clear up some anomalies and also to compare *in situ* electron microscopy results with those obtained by the other techniques.

Experimental Procedures

Specimen Preparation

A stock solution of praseodymium trichloroacetate was prepared (*7*) by dissolving about 10 g of PrO_x in 250 ml of 25% trichloroacetic acid in slight excess. The solution was heated until the onset of precipitation and then cooled. Crystals of trichloroacetic acid were added to the solution until the precipitate just dissolved. Dilution to 300 ml completed preparation of the stock solution.

The praseodymium trichloroacetate was decomposed by heating the solution, saturated with bubbling CO_2 at ambient pressure, at 80–90°C for about 20 min according to the reaction

$$2\ Pr(C_2Cl_3O_2)_3 + 11\ H_2O \rightarrow Pr_2(CO_3)_3 \cdot 8H_2O + 6\ HCCl_3 + 3\ CO_2.$$

The carbonate hydrate was filtered by suction and washed thoroughly with ethanol and then with water until the washings were free of chloride ion as established by the Beilstein test. The precipitate was further washed with ethanol and finally with ether to hasten drying.

The praseodymium hydroxy carbonate [α-$(PrOH)CO_3$] was prepared from the same stock solution as used in the preparation of the hydrate. The filtered solution was heated at 80–90°C for about 2 hr without bubbling CO_2. The precipitate was treated in the same way as was the hydrate.

The Thermogravimetric Study

Thermogravimetric analysis of the decomposition of the specimens was accomplished utilizing a CAHN 1000 electrobalance. The specimens were heated from room temperature to 900°C at a continuous rate of 0.25°C/min in air. The temperature and weight were recorded simultaneously. The precision of the TGA weight changes are estimated to be ±1%.

Specimens for room temperature X-ray analysis were obtained by the following procedure. The lowered furnace was heated at a desired temperature for 2–3 hr. The furnace, at the steady temperature, was then raised to initiate the decomposition reaction. When the recorded temperature and weight were constant the furnace was lowered and set to the next temperature. Each annealed specimen, believed to have been at equilibrium, was removed for X-ray analysis and the process was repeated at the next temperature.

The Room Temperature X-Ray Powder Diffraction Measurements

Diffraction patterns of the samples cooled in the procedure just described were obtained with a Rigaku Geigerflex D/max B diffractometer using monochromatized Cu$K\alpha$ radiation.

The High-Temperature X-Ray Diffraction Study

High-temperature X-ray diffraction patterns were obtained of the decomposition of the two preparations by means of a Rigaku Geigerflex RAD-rA (rotating anode type,

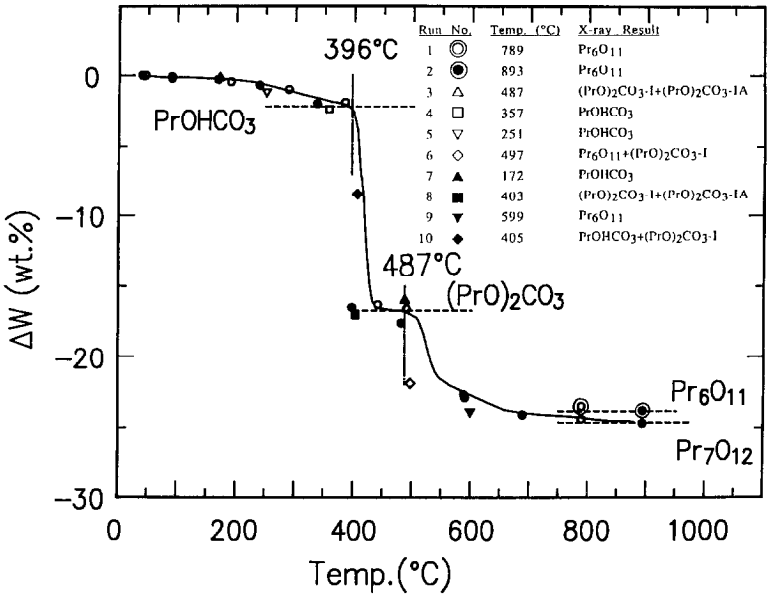

FIG. 1. Thermodynamic observations on α-$(PrOH)CO_3$. The solid line is from continuous heating at 0.25°C/min. Symbols mark equilibrium points from which room temperature powder diffraction patterns indicated the phases present as marked in the inset at the upper right. Horizontal dashed lines mark ideal compositions. Vertical dot-dash lines mark decomposition temperatures.

RU-200A) diffractometer equipped with a CN2311B1 high-temperature attachment.

A powdered sample with ethanol was ground to a paste in a mortar. The paste was applied to the platinum sample holder and the surface made plane by pressing. The sample was heated at 5°C/min to the desired temperature (determined from the TGA curve) and the diffraction pattern was taken after waiting at least 1 hr.

The High-Resolution Electron Microscope Study

Specimens for microscopic study were crushed in an agate mortar to obtain thin crystalline fragments. The powder thus obtained was dispersed in dry ethanol, and a drop of this dispersion was placed on a holey carbon film supported on a copper grid. Crystalline fragments with thin edges favorably dispersed on the grid were observed in the JEM 4000 EX electron microscope equipped with a top-entry double-tilt lift goniometer, operated at 400 kV. The intensity of the electron beam was varied by choosing different spot sizes and/or different condenser apertures. The images were taken using condenser aperture 2 and spot size 3 (8–9 A/cm^2). Successive stages of the reaction were recorded on film and, when profitable, on a video tape. The images were analyzed by measuring the optical diffractograms from suitable areas of the micrographs and comparing these spacings with X-ray diffraction data.

Results

Thermogravimetric Analysis and Room-Temperature Powder X-Ray Diffraction Studies

Figures 1 and 2 present the results of three types of experiments on $(PrOH)CO_3$ and $Pr_2(CO_3)_3 \cdot 8H_2O$, respectively. The continu-

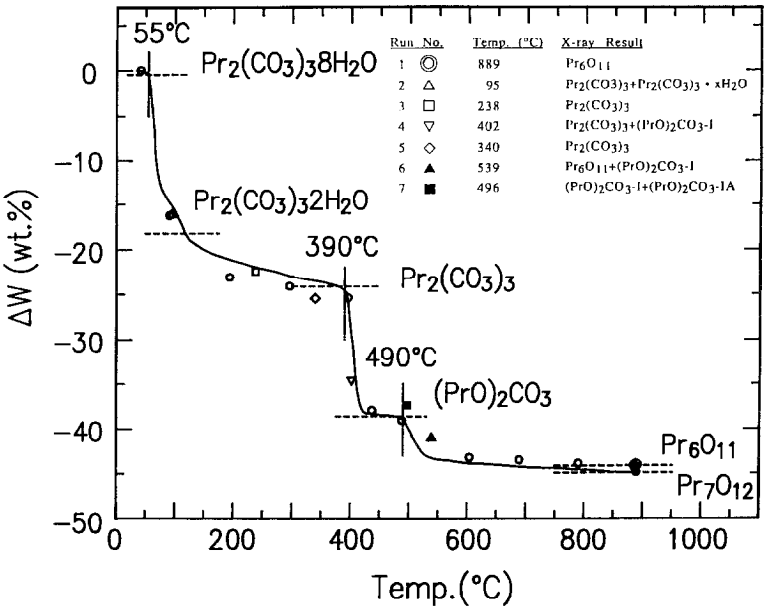

FIG. 2. Thermodynamic observations on $Pr_2(CO_3)_3 \cdot 8H_2O$. The solid line is from continuous heating at 0.25°C/min. Symbols mark equilibrium points from which room temperature powder diffraction patterns indicated the phases present as marked in the inset at the upper right. Horizontal dashed lines mark ideal compound compositions. Vertical dot-dash lines mark decomposition temperatures.

ous curve indicates the weight change of the specimen as a function of temperature which was increasing at a constant rate of 0.25°C/min. The assorted symbols along the curve represent weight changes of the specimen after being annealed for some hours at the corresponding fixed temperature. Some of these materials at equilibrium were examined by X-ray when they had been cooled to room temperature as indicated by run number, temperature, and phase revealed from the X-ray diffraction pattern in the legend in the upper right of the figure. The vertical broken lines mark the decomposition temperature of an existing phase taken as the point where the continuous curve first deviates downward from a straight line. The horizontal dashed lines indicate the calculated weight change of single phase materials. The more or less horizontal regions correspond to the sequence of phases formed as the temperature is increased. The X-ray results reflect any changes that may occur in the specimen during cooling.

Samples from run numbers 3, 8, and 17 were identified as mixtures of orthorhombic $(PrO)_2CO_3$-I (Type-I) and monoclinic $(PrO)_2CO_3$-IA (Type-IA). The transformation of Type-I to -IA and a subsequent transformation of Type-IA to the hexagonal $(PrO)_2CO_3$-II (Type-II) has been reported by Sawyer *et al.* (*8*) for the praseodymium system; however, the latter transformation was not observed in these experiments. (The transformations involving Types I, IA, and II were observed by us in the neodymium system (*6*)). The diffraction maxima in the range of 10 to 50° 2θ are shown in Fig. 3. The final oxide formed by the decomposition in air at about 800°C is known to be Pr_7O_{12} (*9*). The first oxide formed as a virtual state would be the sesquioxide at about 500°C, but it

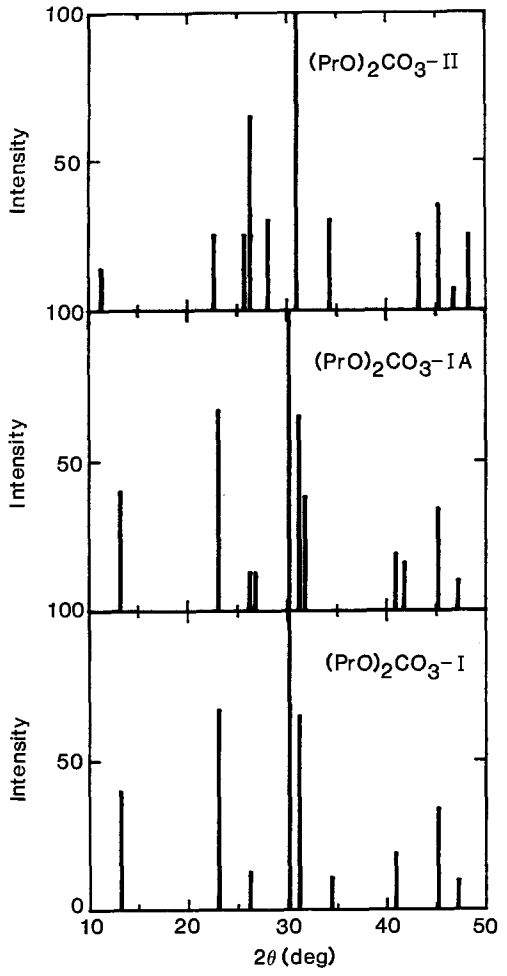

FIG. 3. X-ray diffraction patterns of the polymorphic forms of $(PrO)_2CO_3$.

would oxidize immediately in air to a higher oxide, probably the α phase (PrO_x) of variable composition ($x \simeq 1.8$) (*9*). The $PrO_{1.8}$ formed lost oxygen progressively as the temperature was raised until Pr_7O_{12} was formed at about 800°C. Further reduction did not occur up to the highest temperatures reached in these experiments. The Pr_7O_{12} oxidized as the sample cooled to room temperature, where it would be Pr_6O_{11}. There was no evidence for any stable intermediate carbonates beyond the dioxymonocarbonate.

The High-Temperature X-Ray Powder Diffraction Studies

The *in situ* observation of the decomposition processes and phase reactions of praseodymium hydroxy carbonate and the praseodymium carbonate octahydrate were made using high-temperature X-ray diffraction. Typical results are shown in Figs. 4a and 4b, respectively. In each case the diffraction pattern of the starting material is shown at the bottom with patterns at higher temperatures and at successive stages of decomposition above. The interpreted patterns are summarized in Table I. The small differences between the diffraction patterns of Type-I and Type-IA are illustrated in Fig. 3 (*5*). Our differentiation was based on the peak profiles at about 34 and 42° 2θ. The transition temperatures may differ somewhat from those of the TGA studies since the latter were not varied continuously. The TGA results are likely to be more correct because of the poor thermal geometry of the high-temperature X-ray diffractometer.

The decomposition sequence of the praseodymium hydroxy carbonate, as indicated by the HTXRD study, is as follows:

$$(PrOH)CO_3 \rightarrow (PrO)_2CO_3\text{-I} \rightarrow (PrO)_2CO_3\text{-I} + (PrO)_2CO_3\text{-IA} \rightarrow PrO_x + (PrO)_2CO_3\text{-II} \rightarrow PrO_x \rightarrow Pr_7O_{12}.$$

Notice that no region of single phase Type-IA or Type-II is observed. It must be concluded that Type-I decomposes first to Type-IA but the sequence from there on to the oxide cannot be determined from this study. It is apparent that Type-II is stable at a higher temperature than either of the other two types as has repeatedly been observed (*5*). The sesquioxide decomposition product of the dioxymonocarbonate is surely a virtual state when formed in air since it would

TABLE I

THE STRUCTURES IDENTIFIED IN HIGH-TEMPERATURE X-RAY OBSERVATIONS OF THE DECOMPOSITION OF $(PrOH)CO_3$ AND $Pr_2(CO_3)_3 \cdot 8H_2O$

(1) $(PrOH)CO_3$	
23°C	$(PrOH)CO_3$
230	$(PrOH)CO_3$
408	$(PrOH)_{CO3}$
430	$(PrO)_2CO_3$-I
480	$(PrO)_2CO_3$-I + $(PrO)_2CO_3$-IA
495	$(PrO)_2CO_3$-I + $(PrO)_2CO_3$-IA
511	$PrO_{1.8}$ + $(PrO)_2CO_3$-II
555	$PrO_{1.8-\delta}$ + $(PrO)_2CO_3$-II
708	$PrO_{1.71+\delta}$
863	Pr_7O_{12}
RT	Pr_6O_{11}
(2) $Pr_2(CO_3)_3 \cdot 8H_2O$	
23°C	$Pr_2(CO_3)_3 \cdot 8H_2O$
84	$Pr_2(CO_3)_3 \cdot 2H_2O$ + $Pr_2(CO_3)_3 \cdot 8H_2O$
138	$Pr_2(CO_3)_3$ + $Pr_2(CO_3)_3 \cdot xH_2O$
330	$Pr_2(CO_3)_3$
404	$Pr_2(CO_3)_3$
418	$(PrO)_2CO_3$-I
502	$PrO_{1.83}$ + $(PrO)_2CO_3$-I
502 for 9 hr	$PrO_{1.83}$
756	$PrO_{1.71+\delta}$
903	Pr_7O_{12}
RT	Pr_6O_{11}

oxidize immediately to a higher oxide. As discussed above with the TGA observations and as is apparent from the diffraction patterns, the oxygen composition is higher than in the final product. From previous equilibrium studies (*9*) at a partial pressure of oxygen near that of air and a temperature of about 500°C the oxide should be the disordered α phase of about $PrO_{1.8}$. As the temperature is increased the oxide composition would decrease until at about 700°C it would become $Pr_7O_{12+\delta}$. The composition at 900°C would approach stoichiometric Pr_7O_{12} as clearly shown in the TGA curves. The specimen would be expected to reoxidize to Pr_6O_{11} when cooled in air to room temperature as is observed. This sequence of oxidation, reduction, then reoxidation as the oxide is heated after formation, then cooled to room temperature is clearly apparent in the shift of the peaks in the oxide diffraction patterns to lower, then higher 2θ values.

High-temperature X-ray diffraction observations of the decomposition of the praseodymium carbonate hydrate can be suggested by the sequence

$$Pr_2(CO_3)_3 \cdot 8H_2O \rightarrow Pr_2(CO_3)_3 \cdot xH_2) \rightarrow Pr_2(CO_3)_3 \rightarrow (PrO)_2CO_3\text{-I} \rightarrow PrO_{1.8} \rightarrow Pr_7O_{12} \rightarrow Pr_6O_{11}.$$

FIG. 4. Sequential high-temperature X-ray diffraction patterns beginning with (a) $(PrOH)CO_3$ and (b) $Pr_2(CO_3)_3 \cdot 8H_2O$. Temperatures shown on the left and the decomposition products are identified by the diffraction maxima.

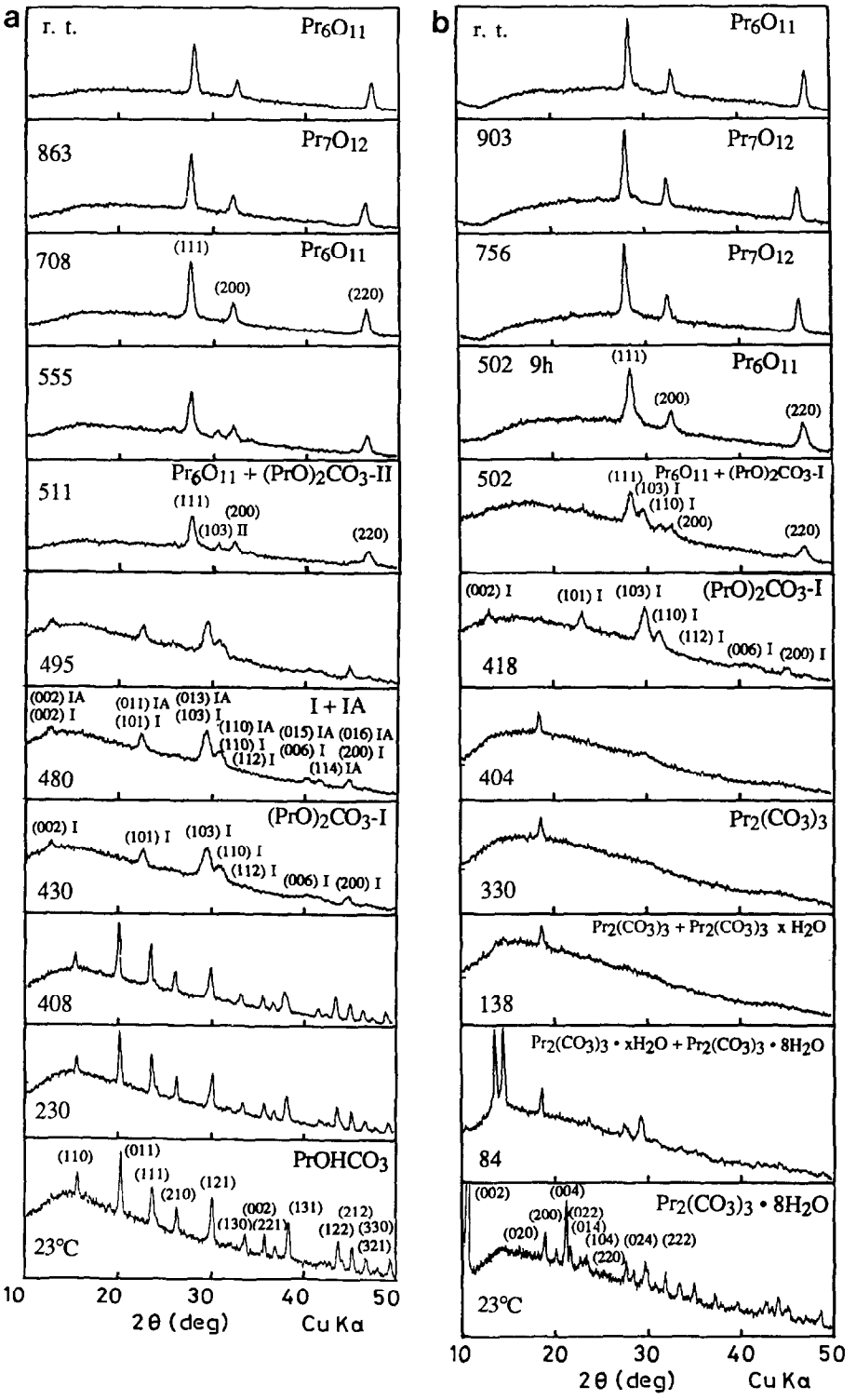
a
r. t.
Pr6O11
863
Pr7O12
708
(111)
(200)
(220)
Pr6O11
555
511
Pr6O11 + (PrO)2CO3-II
(111)
(200)
(103) II
(220)
495
(002) IA
(002) I
(011) IA
(101) I
(013) IA
(103) I
I + IA
(110) IA
(110) I
(112) I
(015) IA
(006) I
(016) IA
(200) I
(114) IA
480
(002) I
(101) I
(103) I
(PrO)2CO3-I
(110) I
(112) I
(006) I
(200) I
430
408
230
(110)
(011)
(111)
(210)
(121)
(002)
(131)
(212)
(130)
(221)
(122)
(330)
(321)
PrOHCO3
23°C
10
20
30
40
50
2θ (deg)
Cu Kα
b
r. t.
Pr6O11
903
Pr7O12
756
Pr7O12
502 9h
(111)
(200)
(220)
Pr6O11
502
(111)
(103) I
(110) I
(200)
(220)
Pr6O11 + (PrO)2CO3-I
(002) I
(101) I
(103) I
(110) I
(112) I
(006) I
(200) I
(PrO)2CO3-I
418
404
Pr2(CO3)3
330
Pr2(CO3)3 + Pr2(CO3)3 x H2O
138
Pr2(CO3)3 • xH2O + Pr2(CO3)3 • 8H2O
84
(002)
(004)
(200)
(022)
(014)
(020)
(104)
(024)
(222)
(220)
Pr2(CO3)3 • 8H2O
23°C
10
20
30
40
50
2θ (deg)
Cu Kα

Most notable is the absence of a transformation of Type-I to Type-IA or Type-II dioxymonocarbonate. Incidentally, this behavior agrees entirely with the HTXRD experience of Turcotte *et al.* (*5*).

There remains some ambiguity in the sequential reactions where PrO_x is formed from $(PrO)_2CO_3$ (Types I, IA, and II). It appears that the path to the oxide can occur from any of the three polymorphic forms of $(PrO)_2CO_3$ and that the actual path and oxide product depend on the kinetics of polymorphic transformations I → IA → II.

High-Resolution Electron Microscopy

1. (PrOH)CO_3. The crystal fragments of $(PrOH)CO_3$ were stable enough to obtain good electron diffraction patterns (Fig. 5a) when irradiated with a low-dose electron beam (2–3 A/cm^2). These fragments decomposed readily with the increased electron beam intensities required for high-resolution imaging. The broad diffuse rings of Fig. 5b are characteristic of highly disordered materials. This observation is a clear indication of a disordered condition resulting from the loss of H_2O and CO_2 before the crystallization of the dioxymonocarbonate.

At higher magnifications a significant amount of specimen vibration was observed during the initial 5–10 min, indicating a vigorous reaction due to the loss of H_2O and CO_2. After the crystal fragment had settled down, it was possible to take some high resolution images (Figs. 6a–6c). A process of nucleation and growth of crystalline material can be observed clearly in these images. The corresponding electron diffraction patterns confirm this condition. Careful measurements of the diffraction patterns (Figs. 5c–5e), lattice fringes, and optical diffraction patterns reveal the crystalline material to be hexagonal dioxymonocarbonate (Type-II) as is to be expected.

A further electron beam irradiation resulted in the nucleation and growth of a new phase. The fragments developed irregular crystalline surface structures (Figs. 7a and 7b). A part of the fragment was aligned with the [110] zone axis of hexagonal Pr_2O_3 (Type-A) parallel to the beam direction (Figs. 8a and 8b). The high resolution images (Figs. 9a and 9b) show the transformation of the hexagonal oxide to the cubic oxide (Type-C). The optical diffraction pattern (Fig. 10) of the regions marked A in Fig. 9a shows the presence of Pr_7O_{12}.

The reaction path as observed here can be written

$$(PrOH)CO_3 \rightarrow (PrO)_2CO_3 \text{ (Type-II)} \rightarrow Pr_2O_3 \text{ (hex)} \rightarrow Pr_2O_3 \text{ (cubic)} \rightarrow Pr_7O_{12} \text{ (rhomb).}$$

This sequence differs from the HTXRD results in that no Type I $(PrO)_2CO_3$ was observed and, of course, the oxide was different since the HTXRD study was carried out in air as was the TGA.

2. $Pr_2(CO_3)_3 \cdot 8H_2O$. Although it was possible to obtain a quick diffraction pattern (Fig. 11a) no good HREM images could be recorded due to the instability of the hydrate. The hydrate lost water readily and transformed into the amorphous carbonate. Crystallization of the dioxymonocarbonate was observed along the edges of the crystal fragment. More than one nucleus of hexagonal dioxymonocarbonate was formed with the *c*-axis lying parallel to the edges of the fragment as was also observed in the case of the hydroxy carbonate.

FIG. 5. A diffraction pattern of $(PrOH)CO_3$ taken (a) after the fragment was oriented along $[1\bar{2}1]$, (b) 2 min after a crystal fragment was found, (c) after 10 min, (d) after 13 min of irradiation with an electron beam of 20 A/cm^2, and (e) after 12 min including five min exposure to an electron beam of 50 A/cm^2. Note how the broad diffuse rings have transformed into rings with sharp spots as a result of decomposition and crystal growth.

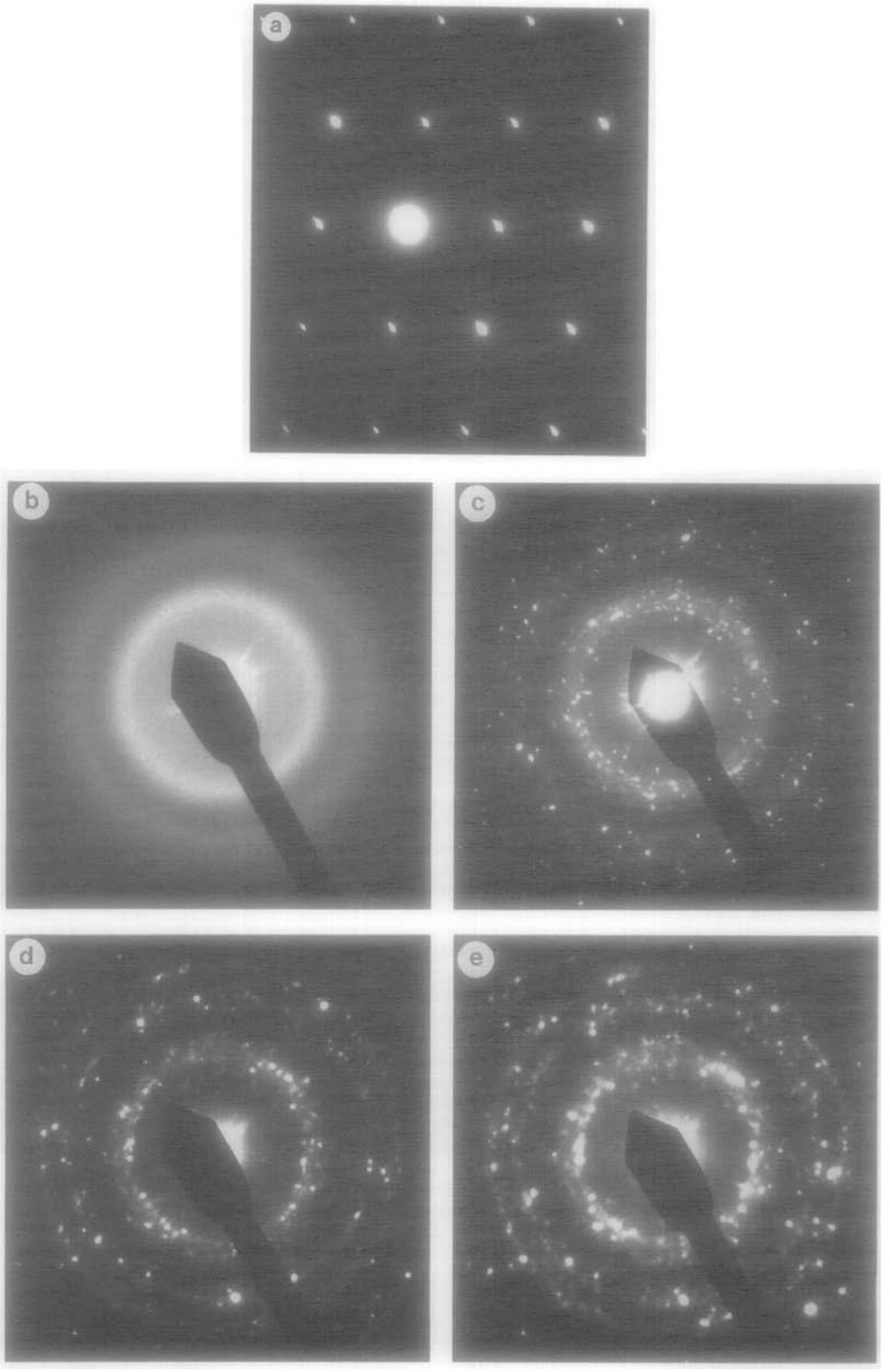
a
b
c
d
e

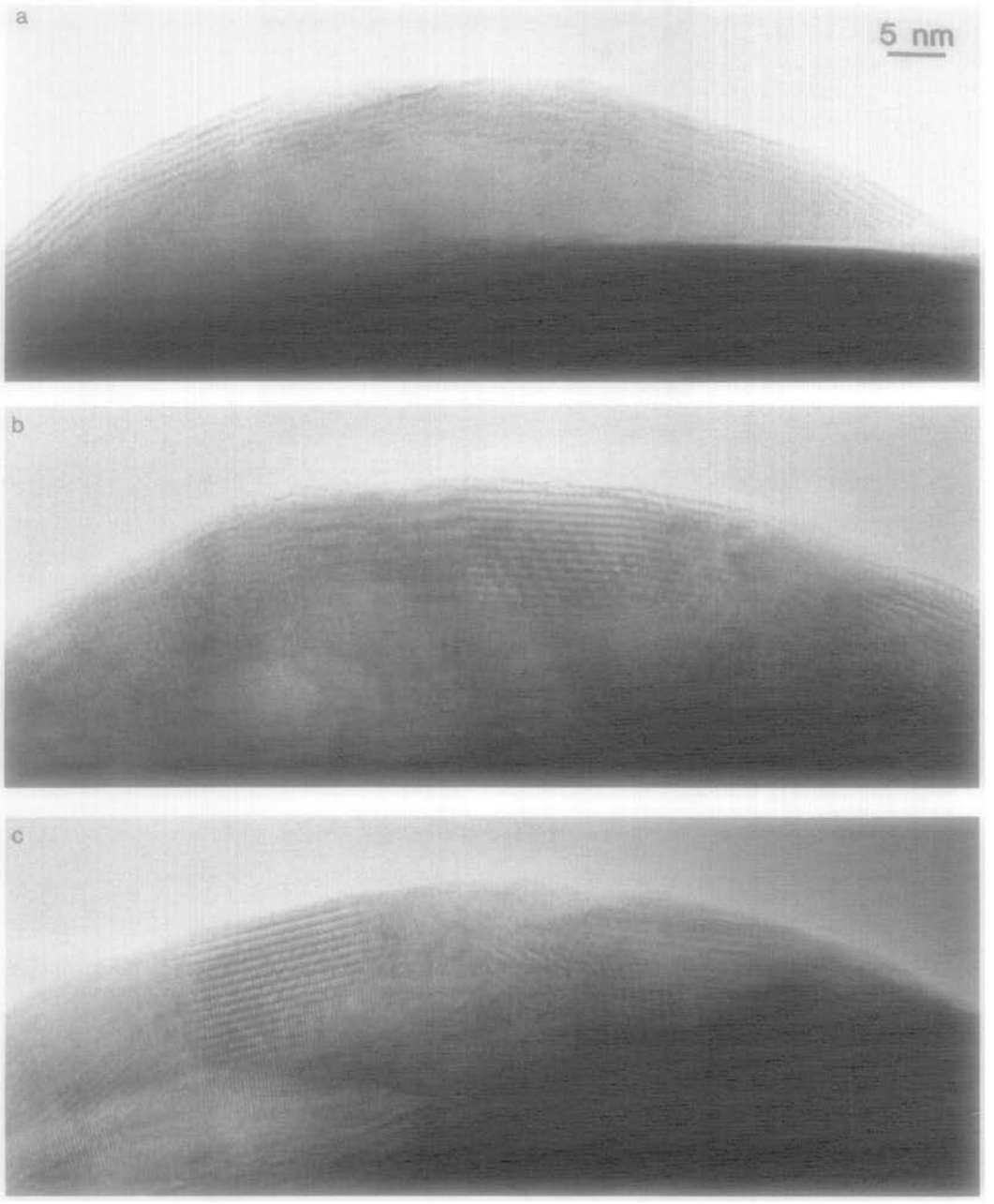

FIG. 6. An HREM image of the same crystal fragment as used in Fig. 5 detailing the stages of crystallization from the edge inward. The time interval between (a) and (b) is 24 min and between (b) and (c) is 2 min during which the specimen was irradiated with a strong beam (50 A/cm^2).

A series of diffraction patterns (Figs. 11a–11c) taken about 20 min apart after intervals of beam heating of 12 and 30 A/cm^2, show the amorphization and then crystallization of the material. The fragment becomes faceted and oxide crystals of about

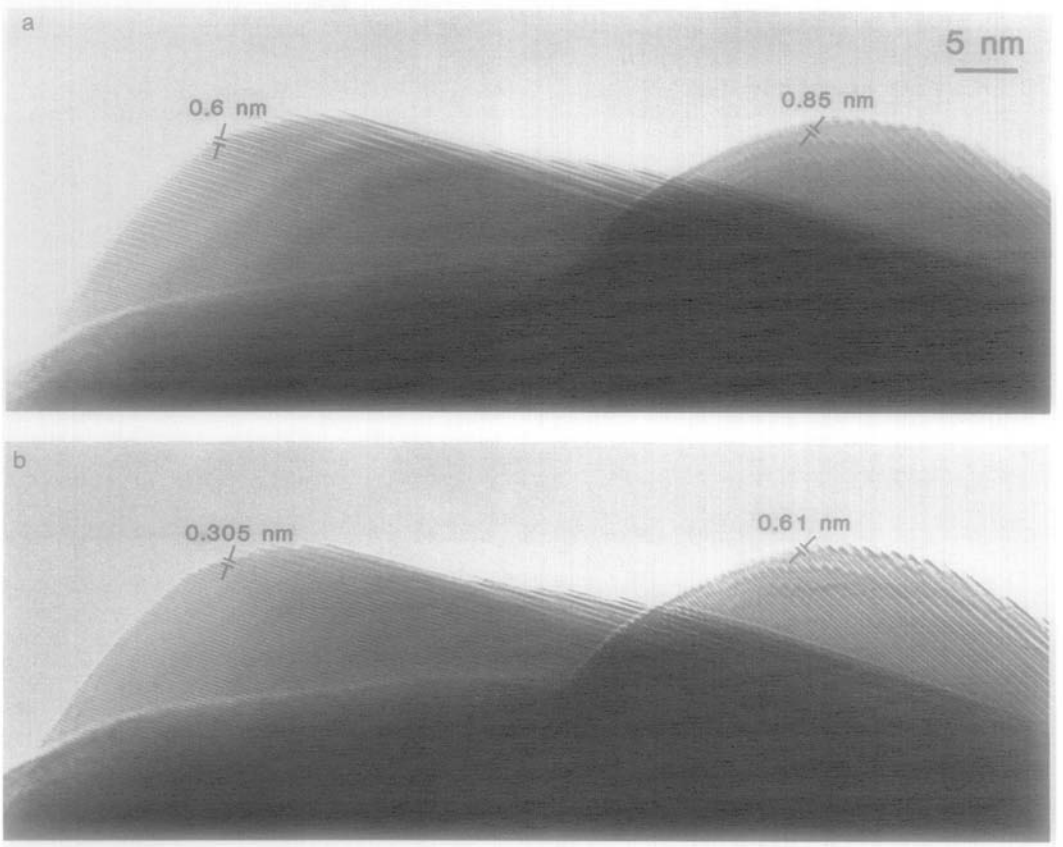

FIG. 7. Another crystal fragment with fringe spacing corresponding to $(PrOH)CO_3$ (0.85 nm), Pr_2O_3 (hex) (0.61 nm), and Pr_2O_3 (cubic, 0.305 nm) in different regions showing a possible sequence of reaction. The fragment was irradiated by a 36 A/cm^2 beam for 2 min between (a) and (b).

30–50 nm are formed. These can be oriented along some axial direction for HREM observation. Figure 12a shows a diffraction pattern from a crystal fragment oriented along the $[10\bar{1}0]$ direction of the hexagonal (A-type) oxide. The crystal fragment was tilted again along one of the axes after about 20 min of beam heating (Fig. 12b). The strong spots of the diffraction pattern can be indexed as C-type Pr_2O_3. As was observed in the hydroxy carbonate, the A-type oxide transformed into C-type (cubic) oxide. The presence of other spots shows that the transformation is not complete as is confirmed by the HREM image shown in Fig. 12c. The two areas marked A and D were identified as hexagonal and cubic oxide phases by indexing the optical diffraction patterns from these regions. After 15 min of electron beam irradiation (24 A/cm^2), the diffraction spots corresponding to the cubic phase became more intense and some weak superstructure reflections appeared (Fig. 12d). The HREM images confirm this observation as most of the fragment is observed to be cubic with layers of hexagonal oxide, marked B and A, respectively, in Fig. 12e. The area marked D was identified as Pr_7O_{12}. The crystal fragment was then tilted along the weak superstructure direction but the weak and incommensurate superlattice spots could not be indexed as Pr_7O_{12} within 1% error (Fig. 12f).

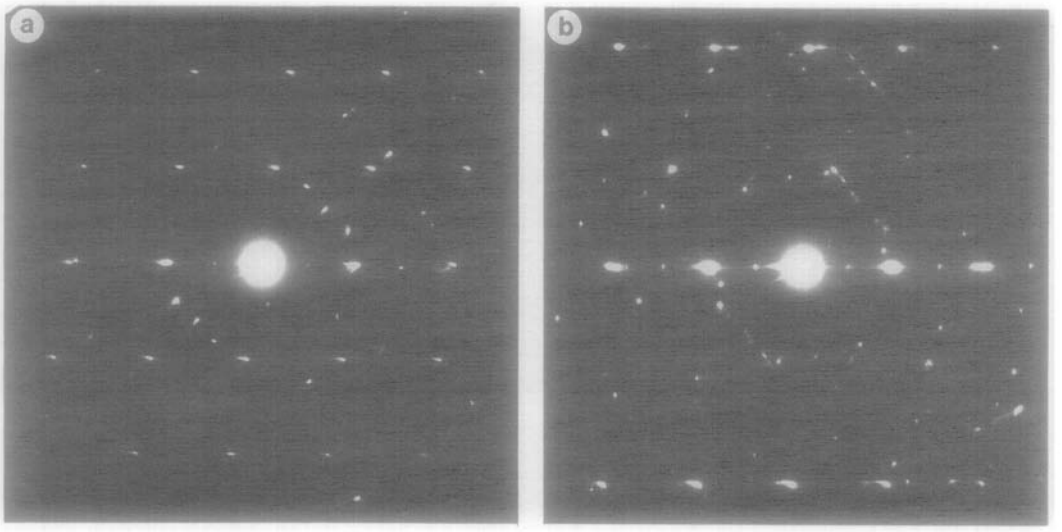

FIG. 8. A diffraction pattern of the crystal fragment from Fig. 3 before (a) and after (b) aligning it along [55101] hexagonal Pr_2O_3.

The reaction sequence observed here by HREM is

$$Pr_2(CO_3)_3 \cdot 8H_2O \rightarrow Pr_2(CO_3)_3 \rightarrow (PrO)_2CO_3 \text{ (Type-II)} \rightarrow Pr_2O_3 \text{ (hex)} \rightarrow Pr_2O_3 \text{ (cubic)} \rightarrow Pr_7O_{12} \text{ (rhomb)}.$$

This sequence differs from the HTXRD results in the form of the $(PrO)_2CO_3$ observed and in the evolution of the oxides formed.

Discussion

It is not uncommon to find a great variation in the listed decomposition temperatures and even the identity of the intermediate compounds in a thermogravimetric experiment. Since the temperature is continuously changed and at different rates one is always to variable degrees away from equilibrium. Furthermore, the ambience of the reaction can be different with each investigation in either pressure or chemical composition. Not least important, the mode of selecting the decomposition temperature from the thermogram is peculiar to each investigator. Nevertheless, some of the reported results from the literature are listed in Table II and hence can be compared. Contrary to our results on the neodymium carbonate study (*6*) the praseodymium dioxymonocarbonate in this study decomposed at the same temperature regardless of its source, presumably because in this instance there was no complication from the formation of a Type-II polymorph.

The structure of $Pr_2(CO_3)_3$ has not been positively detected in these experiments since the X-ray powder diffraction patterns of annealed samples show very few lines. This indicates poor crystallinity of the carbonate consistent with the HREM and electron diffraction observations. The different stages of decomposition observed here are

FIG. 9. (a) A high-resolution micrograph of the crystal fragment from Fig. 7 showing cubic and hexagonal Pr_2O_3. (b) Same area after 40 min of beam radiation.

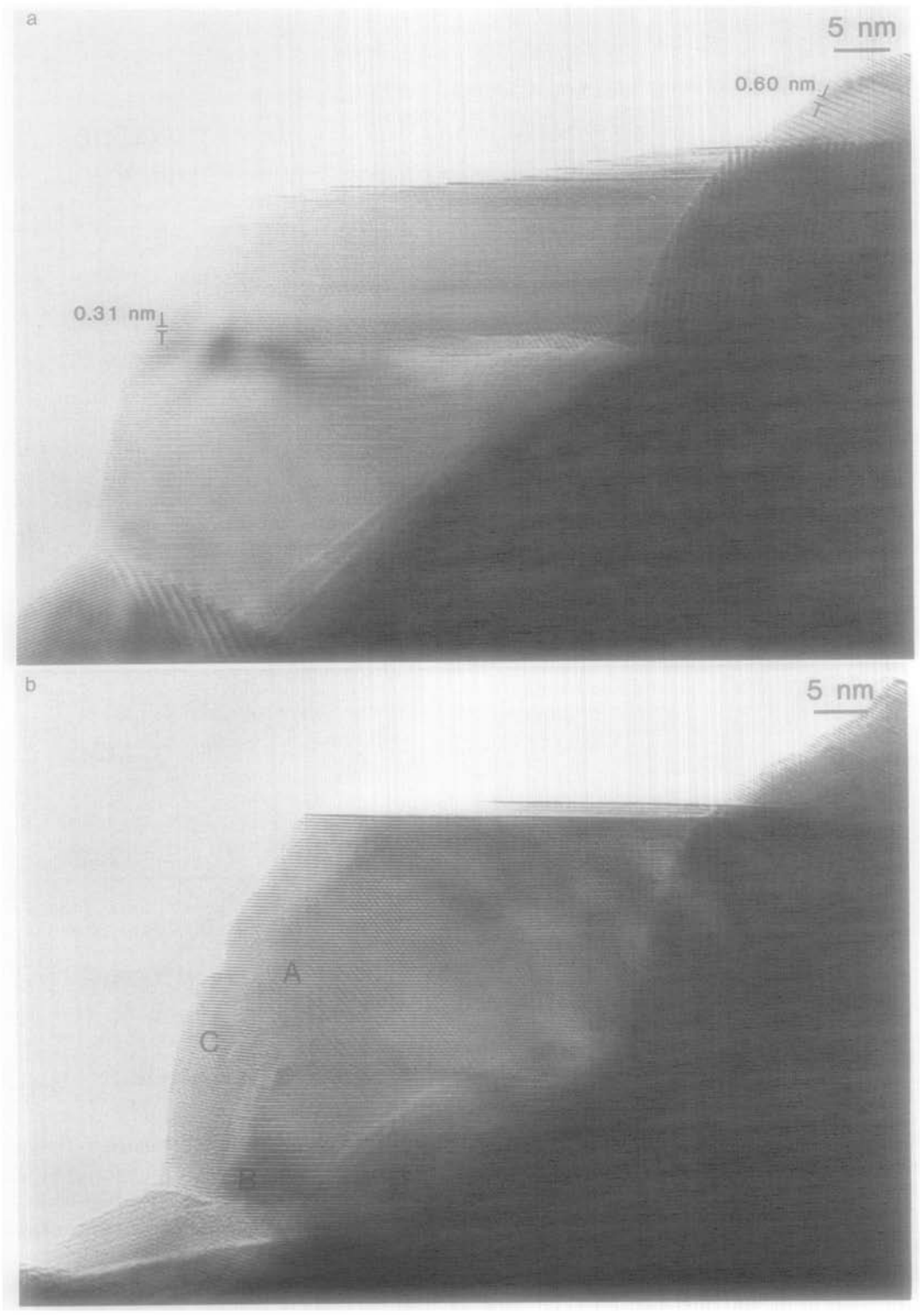
a
5 nm
0.60 nm
0.31 nm
b
5 nm
A
C
B

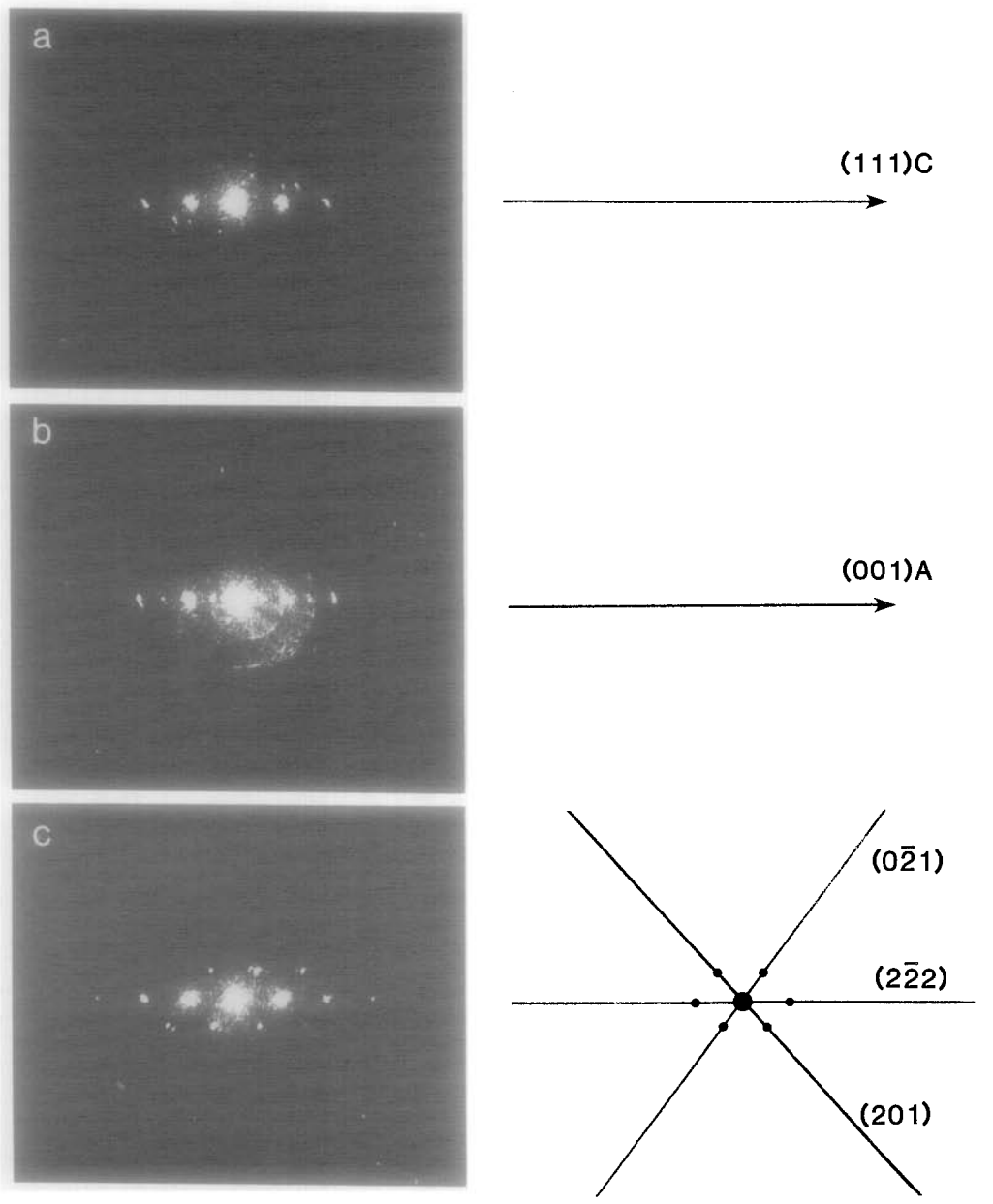

FIG. 10. Optical diffractograms from the areas marked (a) A, (b) B, and (c) C in Fig. 9b.

in agreement with the thermal analysis results except for the final oxide product as outline above. Both the hydroxy carbonate and the carbonate hydrate have layers containing praseodymium and hydroxide ions or water molecules separated by layers of carbonate ions. Therefore, during decomposition the structure must reconstruct in two directions to accommodate the loss of H_2O and CO_2, thus accounting for the highly disordered first phase formed. On the other hand, the structure of the dioxymonocarbonate consists of layers of CO_3^{2-} sandwiched between layers of $(PrO)_n^{n+}$ perpendicular to

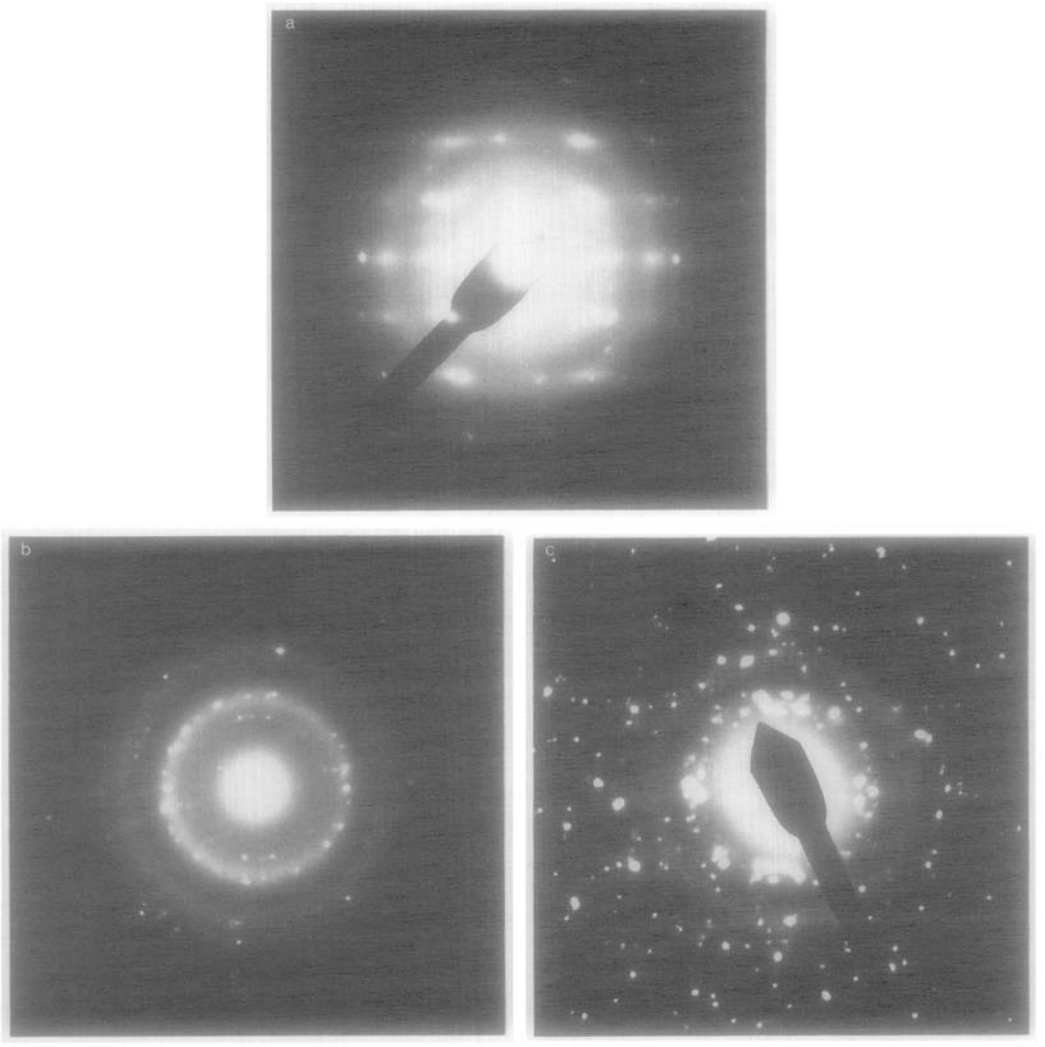

FIG. 11. A diffraction pattern of a crystal fragment taken (a) as soon as it was located. The pattern can be indexed as $Pr_2(CO_3)_3 \cdot 8H_2O$ in the [274] orientation. (b) After 23 min of beam heating (12 A/cm^2). (c) After 20 more min (30 A/cm^2).

the *c*-axis (*10*). During the decomposition of the two forms of dioxymonocarbonate only one-dimensional collapse occurs as CO_2 is lost to form the C-type or A-type oxides and crystallinity is not lost.

The obvious nucleation of dioxymonocarbonate along the edges of the crystal fragments can be explained as follows (see Fig. 6a). The reaction nucleates at a surface from which CO_2 and H_2O are being lost and proceeds inward. Since the crystal fragments are thinner at the edges, crystallization is complete there earlier than in the thicker regions. Once the dioxymonocarbonate is crystallized, further loss of carbon dioxide may be channeled perpendicular to the *c*-axis thus collapsing the structure yielding a shorter and shorter *c*-axis as implied by Fig. 12a. As the reaction proceeds, more and more of the fragment becomes crystallized. The transformation of A-type to C-type involves movement of both oxygen and pra-

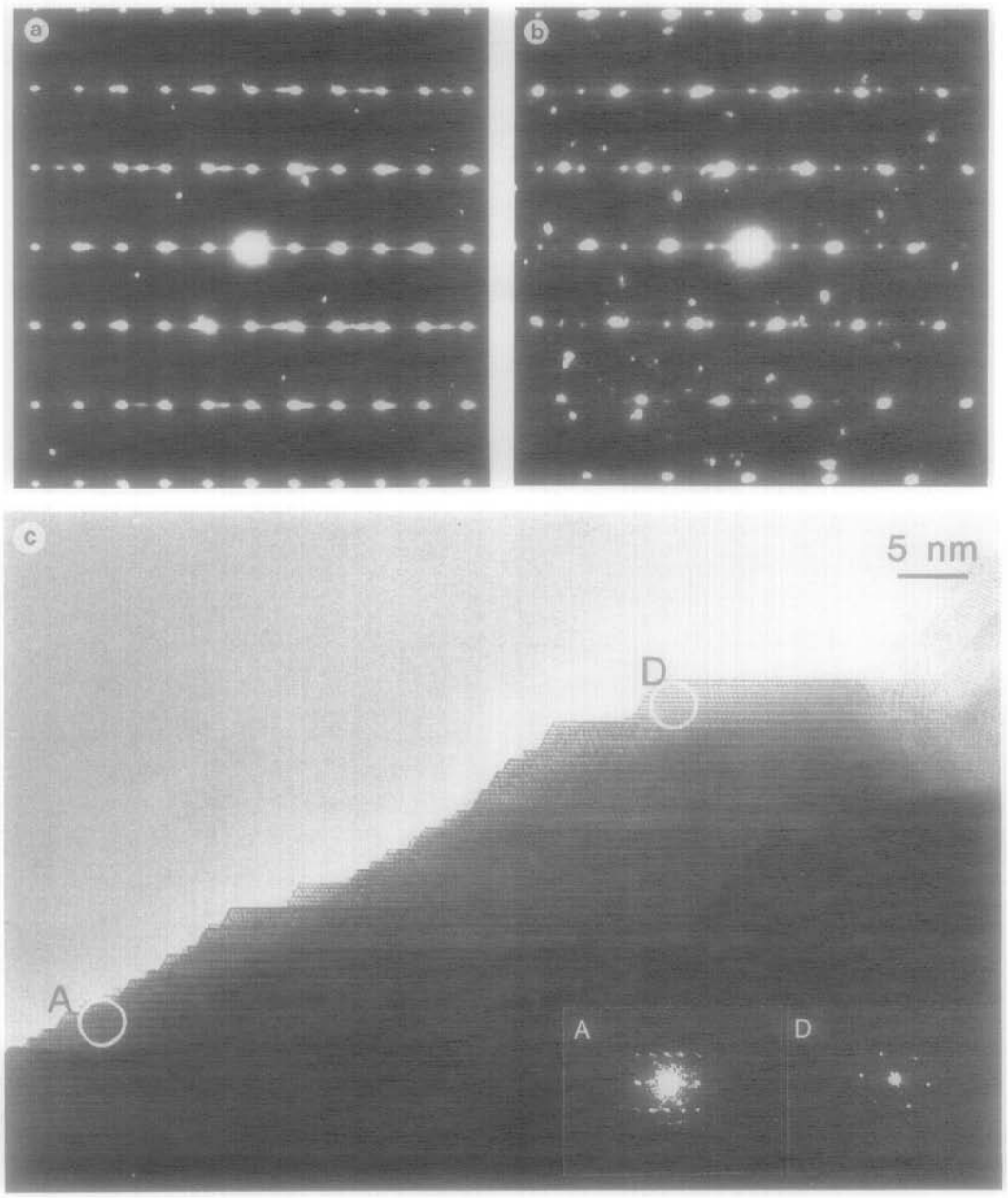

FIG. 12. (a) Diffraction pattern of the crystal fragment used for Fig. 11 oriented along $[10\bar{1}0]$ of Pr_2O_3 (hex). (b) The crystal fragment was oriented again after 20 min of beam heating along [110] of cubic Pr_2O_3. (c) An HREM image and inserted optical diffractogram showing both hexagonal and cubic Pr_2O_3 taken after 30 min (current density = 12 A/cm^2). (d) Diffraction pattern after 15 min of irradiation. (e) Corresponding HREM image showing hexagonal (A), cubic (B), and Pr_7O_{12} regions (D). (f) Diffraction pattern of the same fragment after tilting the crystal fragment along the weak superstructure spots seen in Fig. 12d.

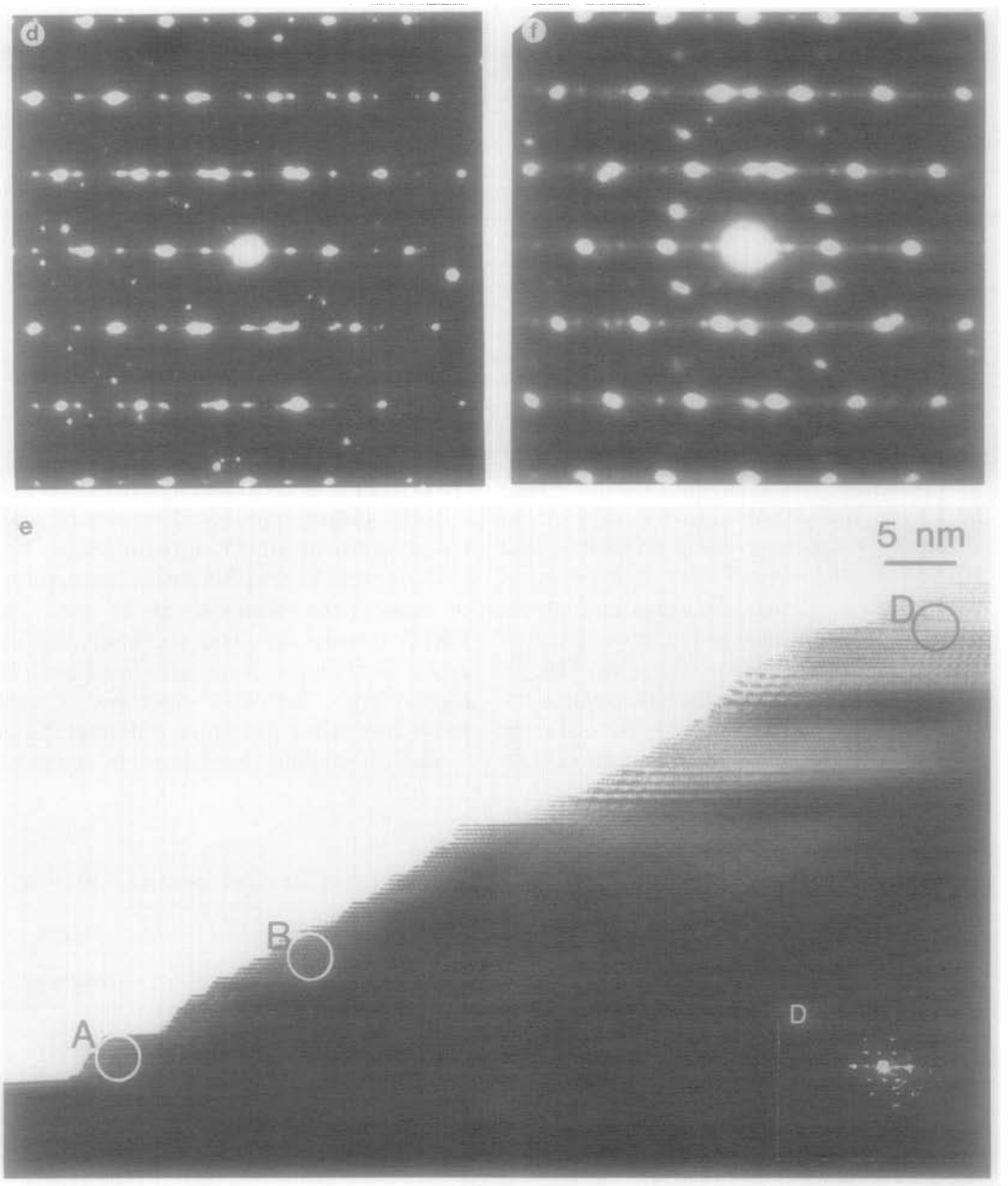

FIG. 12—*Continued*

seodymium atoms in order to change from hexagonal to cubic close packing. This final transformation (hexagonal to cubic) is not observed outside the microscope, hence it must be considered an electron-beam-induced effect.

The TGA runs obtained on specimens decomposed in air reveal only mass changes

TABLE II

THE DECOMPOSITION TEMPERATURES OF $(PrOH)CO_3$ OR $Pr_2(CO_3)_3 \cdot 8H_2O$ AND THEIR DECOMPOSITION PRODUCTS UNDER THE AMBIENT CONDITIONS INDICATED

	$(PrOH)CO_3$	$(PrO)_2CO_3$		Heating rate/ atmosphere
Present study	396°C	487°C		0.25°C/min/air
Charles (5)	390°C	560°C		2°C/min/argon
	$Pr_2(CO_3)_3 \cdot 8H_2O$	$Pr_2(CO_3)_3$	$(PrO)_2CO_3$	
Present study	55°C	390°C	490°C	0.25°C/min/air
Head and Holley (1)		406°C	821°C	0.6°C/min/500 TorrCO_2
Turcotte *et al.* (8)			845°C	~0.5°C/min/CO_2
Sastry *et al.* (3)	60°C	420°C		3–5°C/min/air
Wendlandt and George (7)		510°C	640°C	5°C/min/air

as a function of temperature but they support the more differentiated results of the structurally sensitive XRD, HTXRD, and HREM studies where they can be compared. Table III lists the sequential structures observed in each of the three structurally sensitive methods at the temperatures indicated. In order to rationalize these results it is necessary to keep the different conditions of the experiments in mind. The XRD results are on materials equilibrated at temperature and cooled rapidly to room temperature in air for measurement. The HTXRD results are obtained at temperature on specimens equilibrated in air. The HREM results are from materials decomposed in high vacuum under irradiation by high-voltage, high-flux electrons at relatively low but undetermined temperatures.

There is virtually complete agreement be-

TABLE III

TABULATED OBSERVATIONS OF STRUCTURES IDENTIFIED FROM THREE STRUCTURE-SENSITIVE METHODS

XRD		HTXRD		HREM
Structures	T(°C)	Structures	T(°C)	Structures
		$(PrOH)CO_3$		
$(PrOH)CO_3$-α	357	$(PrOH)CO_3$-α	408	$(PrOH)CO_3$
$(PrOH)CO_3$-α + $(PrO)_2CO_3$-I	405	$(PrO)_2CO_3$-I	430	$(PrO)_2CO_3$-II
$(PrO)_2CO_3$-I + $(PrO)_2CO_3$-IA	487	$(PrO)_2CO_3$-I + $(PrO)_2CO_3$-IA	480	Pr_2O_3-A
Pr_6P_{11} + $(PrO)_2CO_3$-I	497	$PrO_{1.8}$ + $(PrO)_2CO_3$-II	511	Pr_2O_3-C
		$PrO_{1.8}$	708	
Pr_6O_{11}	599	Pr_7O_{12}	863	Pr_7O_{12}(rhomb)
		$Pr_2(CO_3)_3 \cdot 8H_2O$		
		$Pr_2(CO_3)_3 \cdot 8H_2O$	23	
$Pr_2(CO_3)_3$ + $Pr_2(CO_3)_3 \cdot xH_2O$	96	$Pr_2(CO_3)_3 \cdot 8H_2O$ + $Pr_2(CO_3)_3 \cdot xH_2O$	84	$Pr_2(CO_3)_3 \cdot 8H_2O$
$Pr_2(CO_3)_3$	340	$Pr_2(CO_3)_3$	404	Pr_2CO_3
$Pr_2(CO_3)_3$ + $(PrO)_2CO_3$-I	402	$(PrO)_2CO_3$-I	418	$(PrO)_2CO_3$-II
$(Pro)_2CO_3$-I + $(PrO)_2CO_3$-IA	496	$PrO_{1.8}$ + $(PrO)_2CO_3$-I	502	Pr_2O_3-A
		$PrO_{1.8}$	756	Pr_2O_3-C
Pr_6O_{11} + $(PrO)_2CO_3$-I	539			
Pr_6O_{11}	889	Pr_7O_{12}	903	Pr_7O_{12}(rhomb)

tween the XRD and the HTXRD results on $(PrOH)CO_3$. The only discrepancy is that $(PrO)_2CO_3$-II was detected in the HTXRD experiments but not in the XRD preparations, ostensibly because XRD samples were not taken in the temperature range 510 to 560°C where the Type-II appeared in the *in situ* experiments or perhaps the longer annealing period allowed time for decomposition. There is also agreement in the case of the carbonate hydrate except for the lack of detection of the $(PrO)_2CO_3$-IA in the HTXRD results—accountable because of its subtlety in detection. The appearance of Pr_7O_{12} as the high-temperature composition in air is to be expected in the TGA and HTXRD experiments (*9*).

The greater differences between the X-ray and the HREM results are to be understood in terms of the ambient atmosphere—vacuum instead of air—and the likelihood that the temperatures do not reach 300°C in the microscope specimen. Specifically only the $(PrO)_2CO_3$-II polymorph was detected in the decomposition of either compound in the microscope, whereas $(PrO)_2CO_3$-I and -IA were the first products apparent in the X-ray studies. The $(PrO)_2CO_3$-II decomposes topotactically to Pr_2O_3-A, but then this A-type sesquioxide transforms to the C-type, which is the stable form at these low temperatures in the microscope. When the higher oxides of praseodymium are reduced thermally in vacuum above about 600°C, A-type Pr_2O_3 is formed but when reduced with hydrogen at about 550°C or below the C-type is formed in qualitative agreement with microscopic observations. However, the A- to C-type transition in the microscope and finally to the higher oxides has been observed previously with high-flux electron irradiation (*11*). At least two mechanisms for this oxidation in the high vacuum of the microscope must be considered. It would be expected that the electron beam irradiation of adsorbed species from the residual gasses of the microscope column on the specimen surface, e.g., O or OH, would yield active oxidizing species that could oxidize the specimen to a higher oxide. Alternatively there could be beam-induced desorption of PrO(g) producing a vacuum disproportionation resulting in a higher oxide based on C-type Pr_2O_3.

The most striking difference between the X-ray results and those from HREM is that corresponding decompositions can occur at hundreds of degrees lower temperature in the latter, due perhaps to electron-enhance bulk diffusion of H_2O and CO_2, and O from the specimen, and/or polymorphic transformation.

Acknowledgments

It is a pleasure to acknowledge the National Science Foundation who supported this research through research Grant DMR-8820017 and through their support of the high-resolution electron microscope facility via Grant DMR-8611069.

References

1. E. L. Head and C. H. Holley, Jr., *in* "Rare Earth Research II" (K. Vorres, Ed.), Vol. 2, p. 51, Gordon and Breach, New York (1964).
2. R. G. Charles, *J. Inorg. Nucl. Chem.* **27,** 1489 (1965).
3. R. L. N. Sastry, S. R. Yogannrasimhan, P. N. Mehrotra, and C. N. R. Rao, *J. Inorg. Nucl. Chem.* **28,** 1165 (1966).
4. W. W. Wendlandt and T. D. George, *Texas J. Sci.* **13,** 316 (1961).
5. R. P. Turcotte, J. O. Sawyer and L. Eyring, *Inorg. Chem.* **8,** 236 (1969).
6. H. Hinode, R. Sharma and L. Eyring, *J. Solid State Chem.* **84,** 102 (1990).
7. M. L. Salusky and L. L. Quill, *J. Am. Chem. Soc.* **72,** 3306 (1950).
8. J. O. Sawyer, P. Caro, and L. Eyring, *Monatsh. Chem.* **102,** 333 (1971).
9. L. Eyring, *in* "Handbook on the Physics and Chemistry of Rare Earths" (K. A. Gschneidner, Jr., and L. Eyring, Ed.) Vol. 3, p. 358, North-Holland, Amsterdam (1979).
10. A. N. Christensen, *Acta Chem. Scand.* **27,** 1835 (1973).
11. M. Gasgnier, G. Schiffmacher, P. Caro, and L. Eyring, *J. Less-Common Metals* **116,** 31 (1986).